The Journal of Experimental Biology 200, 3119–3131 (1997)
Printed in Great Britain © The Company of Biologists Limited 1997
JEB1112



# THE EFFECTS OF LENGTH TRAJECTORY ON THE MECHANICAL POWER OUTPUT OF MOUSE SKELETAL MUSCLES

GRAHAM N. ASKEW* AND RICHARD L. MARSH†

*Department of Biology, Northeastern University, 360 Huntington Avenue, Boston, MA 02115, USA*

*Accepted 1 October 1997*

## Summary

**The effects of length trajectory on the mechanical power output of mouse soleus and extensor digitorum longus (EDL) muscles were investigated using the work loop technique *in vitro* at 37 °C. Muscles were subjected to sinusoidal and sawtooth cycles of lengthening and shortening; for the sawtooth cycles, the proportion of the cycle spent shortening was varied. For each cycle frequency examined, the timing and duration of stimulation and the strain amplitude were optimized to yield the maximum power output. During sawtooth length trajectories, power increased as the proportion of the cycle spent shortening increased. The increase in power was attributable to more complete activation of the muscle due to the longer stimulation duration, to a more rapid rise in force resulting from increased stretch velocity and to an increase in the optimal strain amplitude. The power produced during symmetrical sawtooth cycles was 5–10 % higher than during sinusoidal work loops. Maximum power outputs of 92 W kg$^{-1}$ (soleus) and 247 W kg$^{-1}$ (EDL) were obtained by manipulating the length trajectory. For each muscle, this was approximately 70 % of the maximum power output estimated from the isotonic force–velocity relationship.**

**We have found a number of examples suggesting that animals exploit prolonging the shortening phase during activities requiring a high power output, such as flying, jet-propulsion swimming and vocalization. In an evolutionary context, increasing the relative shortening duration provides an alternative to increasing the maximum shortening velocity ($V_{max}$) as a way to increase power output.**

Key words: muscle mechanics, power output, skeletal muscle, length trajectory, mouse.

## Introduction

The ability to perform mechanical work and power is a fundamental function of skeletal muscle. Numbers of previous studies have assessed this ability under isotonic or isovelocity conditions. However, many muscles *in vivo* produce power during repetitive contractions that are not adequately described by these measurements. As a result of this problem, investigators have more recently studied muscles during repeated cycles of contraction using the technique illustrated in Fig. 1, which has been variously called the cyclical work or work loop technique (Josephson, 1993). The strength of these studies is that they simultaneously integrate many of the factors that determine muscle performance, including effects that are difficult to model with current information, e.g. activation events, shortening-dependent deactivation and the effects of prestretch. Usually, in the absence of *in vivo* data, the timing and duration of stimulation, and the strain amplitude, are selected to maximize the net power output at a particular cycle frequency. Cycle frequencies appropriate to the muscle's normal activity patterns are usually selected. Such experiments have revealed that muscles generate maximum power output at a particular cycle frequency, above and below which power declines (Altringham and Johnston, 1990; Swoap *et al.* 1993). Net work performed per cycle decreases with increasing cycle frequency. An optimal cycle frequency exists because the work performed at high frequencies declines disproportionately to the increase in cycle frequency (Josephson, 1993).

The effects of varying the length trajectory are not usually included in these studies, most of which have used sinusoidal length trajectories (e.g. Altringham and Johnston, 1990; Swoap *et al.* 1993; Syme and Josephson, 1995). This choice of a standard trajectory provides a convenient comparative framework for examining the performance of different muscles, and for some muscles provides an accurate representation of the *in vivo* strain cycle, e.g. fish swimming (Coughlin *et al.* 1996) and insect flight, within the resolution of the available data (Gilmour and Ellington, 1993; Chan and Dickinson, 1996; Josephson and Ellington, 1997). Where the strain deviates from sinusoidal, *in vivo* recordings of changes in muscle length can be used to replicate the natural mechanical cycle *in vitro* (Marsh *et al.* 1992; Marsh and Olson, 1994; M. Girgenrath and R. L. Marsh, unpublished results). Such studies clearly demonstrate the importance of using

*Present address: Department of Zoology, University of Cambridge, Downing Street, Cambridge CB2 3EJ, UK.
†e-mail: r.marsh@nunet.neu.edu

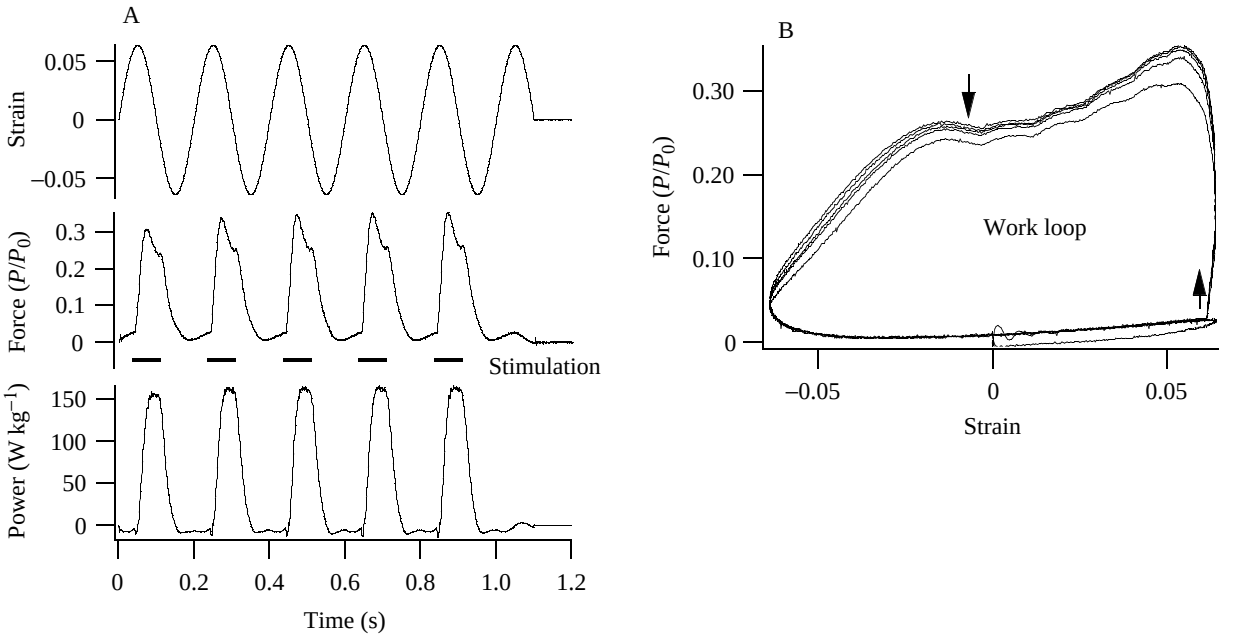


Fig. 1. Illustration of the work loop technique. (A) The top panel shows a record of the sinusoidal length trajectory to which the muscle was subjected, at a cycle frequency of 5 Hz. Five cycles are shown. In the centre panel, the force produced by a mouse soleus muscle undergoing this length trajectory is illustrated. The bars show the period during each cycle when the muscle was stimulated; stimulation began 11 ms before the start of shortening and continued for 65 ms. The lower panel shows the instantaneous power produced during each cycle of work, calculated as the product of force and velocity. The muscle used had a mean fibre length of 8.0 mm at the starting length optimal for work production $L_0$, a wet mass of 5.3 mg and produced a maximum isometric tetanic stress of 28.0 N cm$^{-2}$. (B) Plot of force against strain to produce a series of work loops for the data shown in A at 5 Hz. The work loops are anticlockwise in direction and therefore represent net positive work. The maximum net power output was 46.4 W kg$^{-1}$. The arrows represent the start (↑) and end (↓) of stimulation. $P$, isometric stress; $P_0$, maximal isometric stress during tetanic contractions at $L_0$.

realistic length changes. For example, Marsh and Olson (1994) found that, although the scallop adductor muscle produced similar average power during sinusoidal and natural cycles, the distribution of instantaneous power for each cycle was very different.

An unusual length trajectory has recently been described in the calling muscles of two species of tree frogs (Sarbadhikary and Marsh, 1995; Girgenrath and Marsh, 1997). The strain cycle in these muscles has an asymmetrical sawtooth shape, with shortening lasting longer than lengthening. *In vitro* recordings indicate that these muscles generate approximately twice as much power during simulated natural cycles compared with sinusoidal cycles (M. Girgenrath and R. L. Marsh, unpublished). Josephson (1989) developed a simple mathematical model which predicted that the power output of muscles performing sinusoidal cycles would be 80–90 % of that during symmetrical sawtooth cycles, but he did not consider asymmetrical cycles.

In the present study, we investigated the effects of strain trajectory on the net mechanical power output of mouse extensor digitorum longus (EDL) and soleus muscles. Two types of strain cycle were used: sinusoidal and sawtooth or 'triangular' (where shortening and lengthening occurred at a constant velocity). For the sawtooth cycles, the duration of shortening was varied as a proportion of the total cycle duration. The mouse soleus and EDL muscles were not chosen for this study because they are likely to undergo any of these length trajectories *in vivo*. In fact, muscles during running may produce little mechanical power (Roberts *et al.* 1997). Instead, the results presented here provide the opportunity to examine systematically the effects of length trajectory on two well-characterized mammalian muscles that are predominantly either fast- or slow-twitch. We hypothesized that the enhancement of power seen in the frog muscles during asymmetrical sawtooth cycles is a general feature of skeletal muscle, rather than a specific adaptation of the high-frequency calling muscles of these animals.

The proportion of different fibre types found in the same muscles in the same species of animal varies depending on the strain, sex and age of the individual. For our results to be comparable with future studies, we felt that it was necessary to characterize the fibre type composition of the muscles used in our experiments.

## Materials and methods

### *Muscle mechanics*

Female white mice (strain ICR, Taconic) aged between 4 and 7 weeks were used in all of the experiments. The mean body mass was 26.1±0.4 g ($N$=41).

Animals were killed by cervical dislocation, and the limbs were removed. From each leg, either the soleus or EDL muscle was carefully dissected out at room temperature (approximately 23 °C), in oxygenated Ringer's solution (composition after Daut and Elzinga, 1989). One muscle was used immediately, while the other was pinned at approximately resting length and stored at room temperature, in oxygenated Ringer's solution.

The muscle being used was suspended vertically in a flow-through Perspex chamber filled with circulating, oxygenated Ringer's solution at 37 °C. For both muscles, an aluminium foil clip was attached to the distal tendon, as closely as possible to the muscle fibres without causing damage. This was used to secure the muscle to the lever of an ergometer *via* a light-weight silver chain. The muscle was secured to the base of the chamber by clamping a small piece of bone, attached to the short proximal tendon, using a stainless-steel clip. The muscle was left for at least 30 min to thermoequilibrate and to recover from the dissection.

Muscle force and length were recorded using a servo-controlled ergometer (Cambridge Technology Inc., series 300B). The ergometer was calibrated to yield a length step response time of 1.2 ms to a 1 V, 30 Hz square wave.

After recovery, the muscle length that produced maximum twitch force ($L_{tw}$) was determined using a series of isometric twitches. The muscle was activated using supramaximal stimuli (1 ms pulse width), delivered *via* parallel platinum plate electrodes and amplified using a direct current power amplifier. The electrodes ran the full length of the muscle to ensure uniform activation. A series of isometric tetani was used to ascertain the fusion frequency of the muscle (typically 150 Hz for soleus and 250 Hz for EDL) and also the optimum length for the production of maximum tetanic force ($L_{tet}$). Twitches were characterized by measuring the latency of activation, the time to half-peak force, the time to peak force, the time to half-relaxation and the time to 90 % relaxation; tetani were characterized by measuring the time to half-relaxation. A period of 1 min was allowed between twitches, and 5 min was allowed between tetani, for metabolic recovery.

Following the isometric optimization of length and stimulation parameters, the work loop technique (Josephson, 1985*a*) was used to measure the mechanical power output (Fig. 1A,B). Cyclical length changes were imposed on the muscle, symmetrically about the muscle's starting length. The muscle was activated by supramaximal electrical stimulation such that force was developed during the shortening part of the cycle. By plotting force against length, an anticlockwise 'work loop' was produced, the area of which represented the net work performed by the muscle (Fig. 1B). Multiplying this by the cycle frequency gives the net power output averaged over the whole cycle. Based on James *et al.* (1995), we chose a range of cycle frequencies for each muscle over which positive power could be produced during sinusoidal strain cycles. These frequencies were 1–9 Hz for soleus and 3–17 Hz for EDL. Initially, a series of control sinusoidal work loops was performed to determine the optimum starting length for work production and a control power output. Cycle frequencies of 5 and 11 Hz were used for soleus and EDL, respectively. We selected the duration of the train of stimuli and the strain amplitude that yielded the maximum power output. Muscle length was controlled by SuperScope II (Version 2.1) software operating in a Macintosh IIci computer. Force and length were amplified and recorded by a 12-bit A/D converter with a sampling frequency of 5 kHz. The starting length found to be optimal for work production was used in all subsequent experiments and was defined as $L_0$. A period of approximately 5 min was allowed between each set of work loops to allow time for the muscle to recover.

To determine the effects of strain trajectory on muscle power output, one of four strain patterns was used at each cycle frequency studied: sinusoidal (sin), sawtooth with 25 % of the cycle spent shortening (saw25%), sawtooth with 50 % spent shortening (saw50%) and sawtooth with 75 % spent shortening (saw75%) (Fig. 2). Additional strain trajectories (saw85% and saw95%, abbreviated using similar notation) were performed at cycle frequencies of 5 Hz (soleus) and 11 Hz (EDL). At most frequencies, the muscle was subjected to five cycles of work in each contractile run. At the lowest frequencies, the number of cycles was reduced to one or two to limit fatigue. Work per cycle was calculated by integrating force with respect to length, and net power was calculated using an average of the work

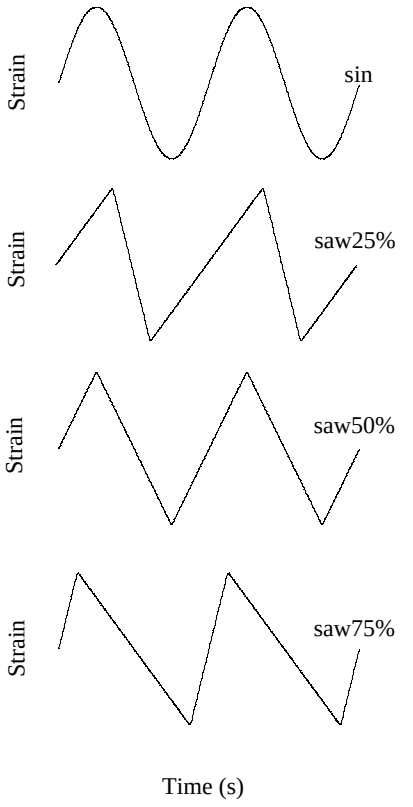


Fig. 2. Examples of some of the length trajectories to which muscles were subjected. (A) Sinusoidal (sin); (B) sawtooth with shortening for 25 % of the cycle (saw25%); (C) saw50%; (D) saw75% (abbreviated using a similar notation).

generated in loops 3–5 (work generated in the first loop was used at low frequencies). At each cycle frequency, the phase of stimulation, the duration of stimulation and the strain amplitude were chosen to give the highest power output, i.e. these were optimized work loops. A series of preliminary experiments was carried out to determine systematically the approximate optimal parameters for power production for all of the different cycle frequencies and length trajectories. Using these as a starting point, each parameter was finely tuned to yield the maximum power output for an individual muscle during the main experiments. In order to monitor the decline in muscle performance, control sinusoidal runs were carried out every fourth or fifth run. We assumed a linear decline in muscle performance between the control runs and corrected our experimental runs to account for the expected decline in power output. Muscle preparations were discarded if the control power output declined below 80 % of the initial power output.

Force–velocity characteristics were determined for a number of muscles using after-loaded, isotonic tetanic contractions. Muscle length was set to $1.05L_0$, and the muscle was maximally stimulated and allowed to shorten across the plateau of the force–length relationship. Tetani were performed at regular intervals to allow correction for the decline in muscle force. A hyperbolic–linear regression equation (Marsh and Bennett, 1986) was fitted to the data using the non-linear curve-fitting routine in the application Igor (Version 3.0, WaveMetrics), and the maximum velocity of shortening ($V_{max}$) estimated by extrapolation to zero force.

### *Fibre length determination*

To determine the mean fibre length relative to the muscle's optimum length, muscles were fixed in 10 % neutrally buffered formalin solution overnight at $L_0$. The connective tissue holding the fibres together was then digested in 30 % nitric acid solution in saline until the fibres fell apart. Digestion was arrested by replacing the nitric acid solution with one containing 50 % glycerol in water. Muscle fibre lengths were determined using an eye-piece graticule, calibrated using a stage micrometer.

### *Histochemical analysis*

Muscles to be fibre-typed were frozen in 2-methylbutane, chilled in liquid nitrogen. Each sample was stored at −70 °C until required for staining. Transverse sections 10 μm thick were cut from each muscle block using a cryostat and mounted on slides. After thawing for 10 min at room temperature, sections were stained for succinate dehydrogenase (SDH) or myosin ATPase activity (with an alkaline preincubation).

Sections stained for SDH activity were incubated for 30 min at 37 °C in a solution of 0.1 mol $l^{-1}$ phosphate buffer (pH 7.6), 0.1 mol $l^{-1}$ sodium succinate and 0.61 mmol $l^{-1}$ nitroblue tetrazolium (after Nachlas *et al.* 1957). After rinsing in distilled water, slides were briefly (1–2 s) immersed in a 0.1 % aqueous solution of safranin, rinsed again in water, and air-dried. Finally, the sections were mounted in Aqua-mount. Fibres were classified dichotomously into those containing high SDH activity (i.e. types I and IIa ) and those containing very low SDH activity (type IIb).

The demonstration of myofibrillar ATPase was based on the methods of Padykula and Herman (1955) and Chayen and Bitensky (1991). Sections were immersed for 7 min at 37 °C in an alkaline preincubation solution of 0.2 mol $l^{-1}$ glycine and 0.018 mol $l^{-1}$ $CaCl_2$, buffered to pH 9.4. This was followed by incubation for 20 min at 37 °C in a reaction medium containing 0.018 mol $l^{-1}$ $CaCl_2$, 0.1 mol $l^{-1}$ Tris and 2.7 mmol $l^{-1}$ ATP (pH 9.4). Slides were then washed in three changes of 1 % $CaCl_2$ solution, incubated in 2 % cobalt chloride solution for 2 min, rinsed in three changes of 0.1 mol $l^{-1}$ Tris, and placed in a 1 % solution of ammonium sulphide for 30 s. After rinsing in distilled water, sections were mounted in Aqua-mount. Fibres showing high alkaline ATPase activity were assumed to be fast (i.e. types IIa and IIb); fibres showing low activity were assumed to be slow (type I).

For both EDL and soleus, positive and negative staining were recorded in a sample of approximately 300 fibres from each muscle section. By combining the results from the two staining techniques, the proportions of each fibre type were determined. The application NIH Image (Version 1.57) was used to digitize a sample of muscle fibres from each section in order to determine the relative cross-sectional areas occupied by each fibre type.

## Results

All results presented are mean ± standard error of the mean (S.E.M.), for five replicates, unless stated otherwise.

### *Isometric properties*

Table 1 summarizes the mechanical and physical properties of mouse soleus and EDL muscles. The maximum isometric tetanic stresses $P_0$ for the two muscles were similar and comparable to previously measured values (e.g. Luff, 1981; James *et al.* 1995). The force rise-time was approximately half as long in EDL as in soleus muscle.

The effects of starting length on isometric twitch and tetanic force are shown in Fig. 3. The length at which twitch force was maximal ($L_{tw}$) was approximately 8 % longer than that yielding peak tetanic force ($L_{tet}$). Similar results have been found in other muscles, where the optimum length for maximum twitch force is usually 5–10 % longer than for the tetanus (Rack and Westbury, 1969; Close, 1972).

### *Work loops using different length trajectories*

The muscle length which yielded the maximum work output during control loops ($L_0$) was the same as that at which peak tetanic force was measured (Fig. 3). For both muscles, this was, on average, 7 % less than $L_{tw}$. Similar findings have previously been reported for a crab respiratory muscle (Josephson and Stokes, 1989) and rat papillary muscles (Layland *et al.* 1995).

For each of the strain patterns used for both soleus and EDL, there was a distinct, optimal cycle frequency at which net

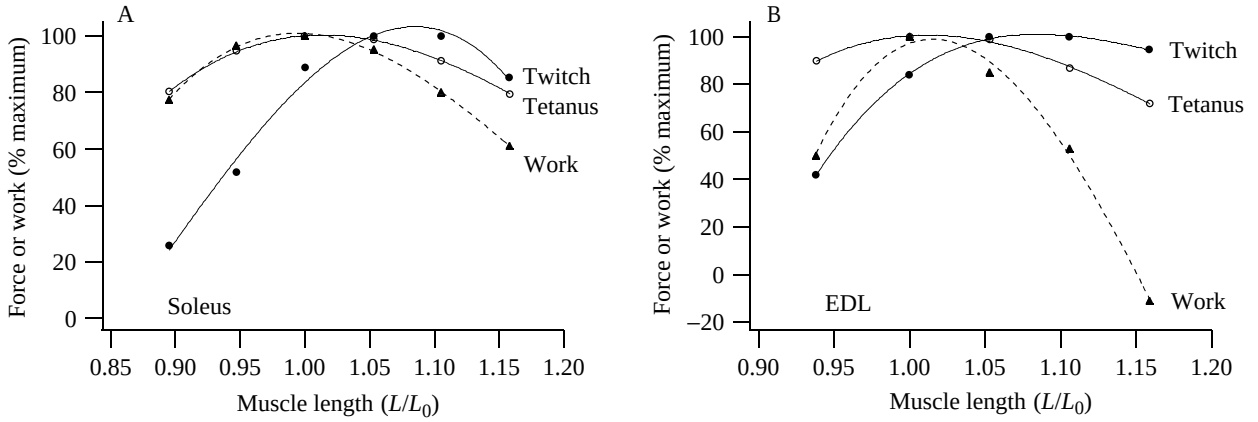


Fig. 3. The effects of starting length on twitch force, tetanic force and work output for individual mouse soleus (A) and EDL (B) preparations. Soleus: mass 5.2 mg; mean fibre length 8.4 mm at $L_0$; isometric stress 25.7 N cm$^{-2}$. EDL: mass 7.0 mg; mean fibre length 6.4 mm at $L_0$; isometric stress 19.0 N cm$^{-2}$.

Table 1. *Isometric and isotonic properties of soleus and EDL muscles*

| | Soleus | EDL |
|---|---|---|
| $P_0$ (N cm$^{-2}$) | 26.9±0.7 (18) | 24.3±0.8 (23) |
| Twitch:tetanus ratio | 0.12±0.01 (18) | 0.11±0.01 (23) |
| Latency (ms) | 1.6±0.1 (18) | 1.3±0.1 (23) |
| Twitch half-rise time (ms) | 4.3±0.2 (18) | 2.3±0.1 (23) |
| Twitch rise time (ms) | 16.2±0.4 (18) | 7.3±0.2 (23) |
| Twitch half-relaxation time (ms) | 23.0±1.0 (18) | 9.1±0.4 (23) |
| Twitch 90 % relaxation time (ms) | 58.5±2.6 (18) | 25.5±1.3 (22) |
| Tetanic half-relaxation time (ms) | 41.6±2.3 (15) | 12.5±.4 (20) |
| Muscle mass (mg) | 5.6±0.2 (18) | 7.0±0.2 (23) |
| Muscle length, $L_0$ (mm) | 9.8±0.2 (18) | 10.7±0.2 (23) |
| Mean fibre length ($L/L_0$) | 0.85 | 0.55 |
| $V_{max}$ ($L$ s$^{-1}$) | 6.0±0.3 (4) | 14.1±0.8 (4) |
| $P/P_0$ at maximum power | 0.38±0.02 (4) | 0.44±0.01 (4) |
| $V/V_{max}$ at maximum power | 0.22±0.01 (4) | 0.26±0.01 (4) |
| $\dot{W}_{max}$ (W kg$^{-1}$) | 126.4±8.0 (4) | 372.4±31.6 (4) |
| Power ratio, $\dot{W}_{max}/P_0V_{max}$ | 0.08±0.002 (4) | 0.12±0.004 (4) |

$P_0$, maximal isometric stress during tetanic contractions at $L_0$; $L$, mean fibre length; $L_0$, the muscle length at which cyclical power output (and tetanic force) are maximal; $V$, velocity of shortening; $V_{max}$, maximum velocity of shortening as predicted from the force–velocity curve; $\dot{W}_{max}$, maximum isotonic power output. The power ratio was calculated after conversion of $\dot{W}_{max}$, $V_{max}$ and $P_0$ to S.I. units (W, N and m s$^{-1}$) for a unit volume of muscle.

Values are means ± S.E.M. ($N$).

Table 2. *Maximum power output measured for soleus and EDL muscles using different length trajectories*

| | | Net power output (W kg$^{-1}$) | Cycle frequency (Hz) | Strain amplitude (%) | $V/V_{max}$ |
|---|---|---|---|---|---|
| Soleus | Sinusoidal | 51.3±1.8 | 3.3 | ±8 | 0.18 |
| | saw25% | 28.7±1.3 | 2.3 | ±6 | 0.18 |
| | saw50% | 54.56±2.3 | 3.5 | ±8 | 0.19 |
| | saw75% | 76.4±3.7 | 4.1 | ±11 | 0.20 |
| EDL | Sinusoidal | 132.2±7.7 | 8.8 | ±6 | 0.15 |
| | saw25% | 82.7±6.1 | 5.2 | ±6 | 0.18 |
| | saw50% | 141.7±7.2 | 8.8 | ±6 | 0.15 |
| | saw75% | 196.7±9.5 | 9.4 | ±8 | 0.14 |

$V$, velocity of shortening; $V_{max}$, maximum velocity of shortening as predicted from the force–velocity curve. $V/V_{max}$ reported for the sinusoidal length trajectory is the mean shortening velocity. The trajectories were either sinusoidal on sawtooth (see text and Fig. 2).

Values are means ± S.E.M., $N$=5.

power output was maximal (Fig. 4). Maximum power outputs ranged from 29 W kg$^{-1}$ (saw25%) to 79 W kg$^{-1}$ (saw75%) for soleus, and from 83 W kg$^{-1}$ (saw25%) to nearly 200 W kg$^{-1}$ (saw75%) for EDL. The power outputs produced during sinusoidal and saw50% cycles were similar, although for both muscles power was typically 5–10 % greater during the sawtooth trajectory. The net power outputs obtained using sinusoidal strains were 51.3 W kg$^{-1}$ for soleus and 132.2 W kg$^{-1}$ for EDL muscle. Power output was found to increase for both muscles as the proportion of the cycle spent shortening increased (Fig. 4).

When shortening duration was extended beyond 75 % at frequencies nearly optimal for each muscle, power output rose further. The maximum power outputs obtained during cyclical contractions were 92 W kg$^{-1}$ (soleus at 5 Hz) and 247 W kg$^{-1}$ (EDL at 11 Hz) using saw85% and saw95% strain trajectories, respectively. This represented approximately 70 % of the maximum isotonic power output for each muscle (Fig. 5).

The cycle frequency yielding the maximum power output increased as the proportion of the cycle spent shortening increased (Fig. 4; Table 2). A cycle frequency of 5.2 Hz yielded the maximum power output for EDL performing saw25% cycles, and this increased to approximately 9.4 Hz using a saw75% cycle (Fig. 4; Table 2). There was a smaller

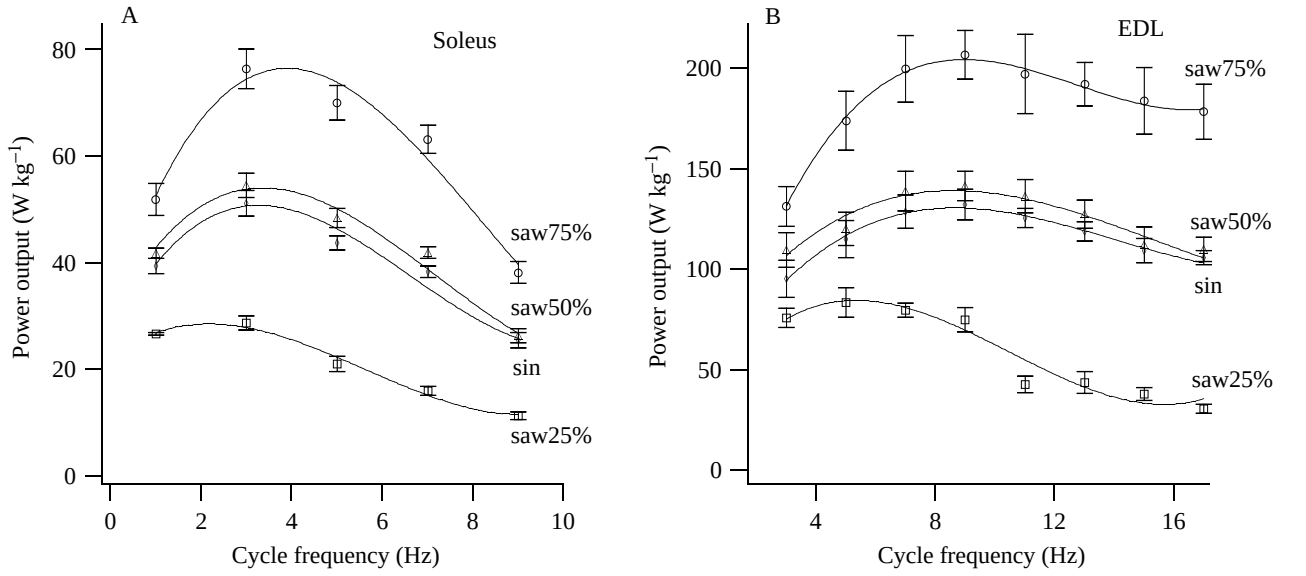


Fig. 4. Mechanical power output of mouse soleus (A) and EDL (B) preparations as a function of cycle frequency for different imposed length trajectories. Data represent mean ± S.E.M., $N \geqslant 5$. The lines are fourth-order polynomials, fitted using a least-squares regression.

difference between the optimal cycle frequency comparing saw50% with saw75% length trajectories than there was comparing saw25% and saw50% cycles (Fig. 4; Table 2). The relationship was less clear for soleus and was very dependent on the curve-fitting procedure used; however, a similar trend is observed. For soleus, the optimum cycle frequency increased from 2.3 Hz (saw25%) to 4.1 Hz (saw75%) (Fig. 4; Table 2; estimated from the fitted polynomial regression).

For each strain trajectory, there was an optimal strain amplitude. Net power output declined at strain amplitudes below or above this optimum (Fig. 6A). An optimum strain amplitude for power output has been reported in many different muscles and seems to be a general feature of all muscles (Josephson and Stokes, 1989). The optimum strain amplitude was found to increase as the proportion of the cycle spent shortening increased (Fig. 6A).

We also noted that, as the cycle frequency increased, the optimal strain amplitude, the optimal stimulation duration and the work measured per cycle all decreased as in previous work loop studies (Josephson, 1993; James *et al.* 1995).

Work loop shapes differed greatly between sinusoidal and sawtooth length trajectories (Fig. 7). However, the overall shape of the work loops produced using sawtooth cycles with differing proportions of shortening did not change dramatically. Sinusoidal work loops had highest forces at the peak length (and also at the minimum length at low cycle frequencies) (Fig. 7). Sawtooth work loops at low cycle frequencies tended to attain peak force midway through shortening. At higher frequencies, the force was much lower at the end of shortening, presumably because the muscle was deactivating and relaxing (Fig. 7).

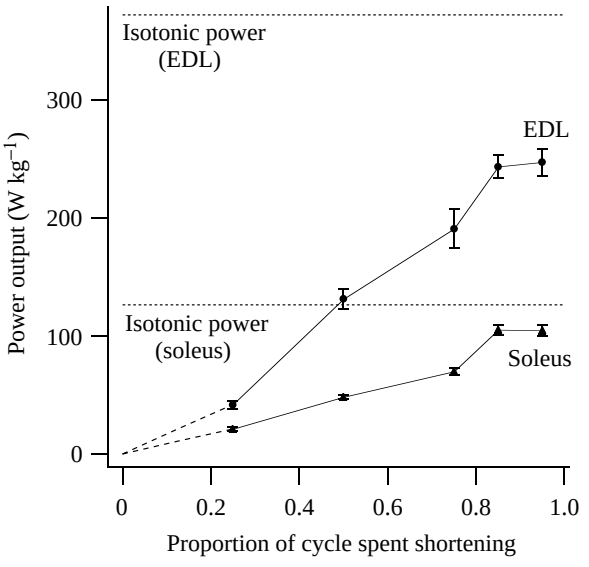


Fig. 5. The effects of the proportion of the cycle spent shortening on the power output of the soleus operating at 5 Hz and the EDL operating at 11 Hz. Data represent means ± S.E.M. (five muscles). The maximum isotonic power output (see Table 1) of each muscle is indicated by the horizontal, broken line.

### *Force–velocity muscle properties compared with cyclical contractions*

A hyperbolic–linear equation was fitted to the force–velocity data obtained during afterloaded contractions (Marsh and Bennett, 1986). Extrapolation of this equation to zero force was used to obtain estimates of the maximum shortening velocity $V_{max}$ of the muscle fibres. $V_{max}$ for soleus was $6.0\,L\,s^{-1}$ and $V_{max}$ for EDL was $14.1\,L\,s^{-1}$, where $L$ is fibre length (Fig. 8; Table 1). In determining $V_{max}$, we did not correct for the angle subtended between the muscle fibres and the long axis of the muscle. The error caused by this omission is less than 0.1 % for these muscles (Close, 1964). From the force–velocity

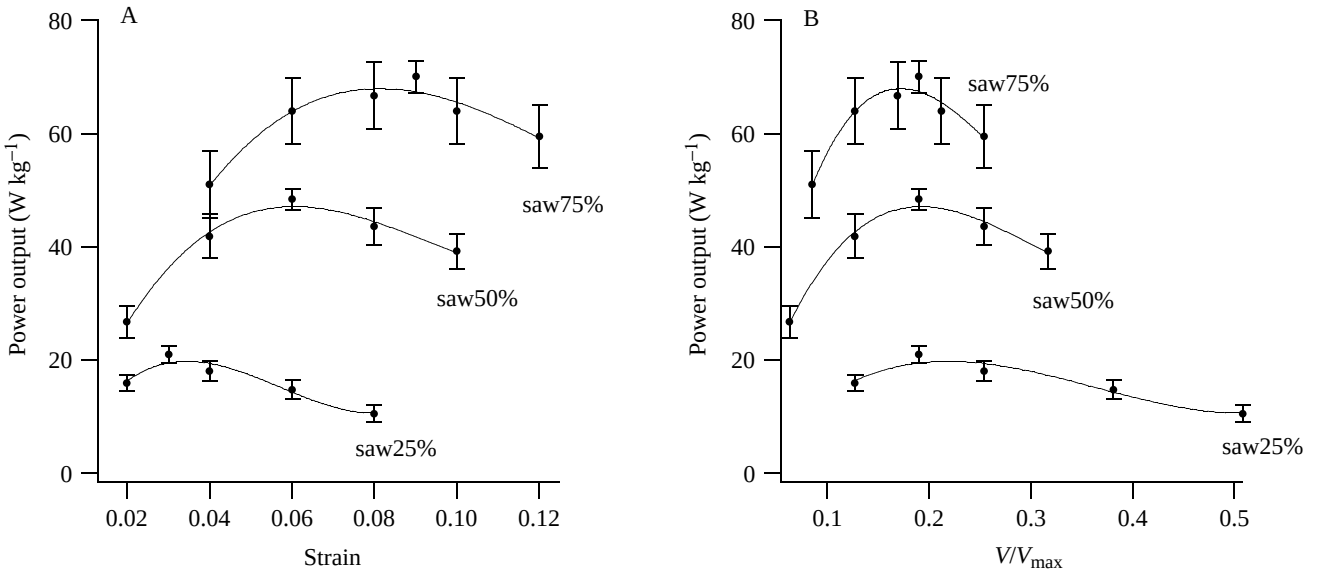


Fig. 6. The effects of strain amplitude and shortening velocity on power output. (A) The power output of mouse soleus operating at a cycle frequency of 5 Hz during saw25%, saw50% and saw75% length trajectories (see Fig. 2) is plotted as a function of strain amplitude. (B) The effects of $V/V_{max}$ on power output using the same data as plotted in A. $V/V_{max}$ was estimated using individual $V$ values and the mean $V_{max}$. Symbols represent mean ± S.E.M. for five muscles; the lines are third-order polynomials, fitted using a least- squares regression.

relationship, the instantaneous power output was estimated to be 126.4 W kg$^{-1}$ in soleus and 372.4 W kg$^{-1}$ in EDL (Table 1). The velocity at which power was maximal was $0.22V_{max}$ and $0.26V_{max}$ in soleus and EDL, respectively (Table 1). The stress at peak isotonic power $P_0$, was 0.38 N cm$^{-2}$ (soleus) and 0.44 N cm$^{-2}$ (EDL) (Table 1).

During sinusoidal work loops, the muscles were found to operate close to the force–velocity curve during only part of the shortening phase of the length cycle (Fig. 8). As cycle frequency increased, the muscles operated on their force–velocity curves for a smaller proportion of the shortening duration. For example, soleus at 1 Hz operated on the force–velocity curve for approximately 80 % of the shortening duration, whereas at 9 Hz this proportion decreased to 14 % (Fig. 8A). EDL operated close to the force–velocity curve for approximately 55 % of the shortening duration at 5 Hz and 9 % of the shortening duration at 17 Hz (Fig. 8). Forces developed during sinusoidal work loops did not exceed the force–velocity relationship by more than 10 %.

Table 3. *Fibre types of soleus and EDL muscles based on histochemical demonstration of succinate dehydrogenase and alkaline myosin ATPase activities*

| | Fibre type | Relative number (%) | Relative proportion (%) |
|---|---|---|---|
| Soleus | Type I | 47.2±1.6 (6) | 65.6±2.0 (6) |
| | Type IIa | 52.8±1.6 (6) | 34.4±2.0 (6) |
| | Type IIb | 0 | 0 |
| EDL | Type I | 0 | 0 |
| | Type IIa | 46.4±2.0 (6) | 32.6±2.0 (6) |
| | Type IIb | 53.6±2.0 (6) | 67.4±2.0 (6) |

Values are means ± S.E.M. (*N*).

### *Fibre typing*

The results from the histochemical staining are shown in Table 3. Soleus contained approximately equal numbers of fast oxidative glycolytic (FOG, type IIa) and slow oxidative (SO, type I) fibres; however, owing to the differences in size between these two fibre types, the SO fibres occupied 65.6 % of the physiological cross-sectional area of the muscle fibres. The EDL contained similar numbers of type IIb and IIa fibres but, owing to their larger size, the type IIb fibres occupied 67.4 % of the fibre's cross-sectional area.

## Discussion

### *Muscle performance in relation to previous studies and fibre type composition*

A number of parameters of muscle performance measured in this study differ slightly from those measured previously for mouse muscle. For example, although we measured similar or slightly higher stresses compared with those found by Luff (1981), our values for $V_{max}$ (6.0 $L$ s$^{-1}$ and 14.1 $L$ s$^{-1}$ for soleus and EDL, respectively) were somewhat lower than those measured by him (8.6 $L$ s$^{-1}$ and 16.3 $L$ s$^{-1}$ for soleus and EDL, respectively). Luff's (1981) estimates of maximum isotonic power are correspondingly higher than ours. However, the values measured in the present study for average mechanical power during sinusoidal work loops were 30–50 % higher than those previously measured (James *et al.* 1995).

Unfortunately, evaluating these differences is difficult

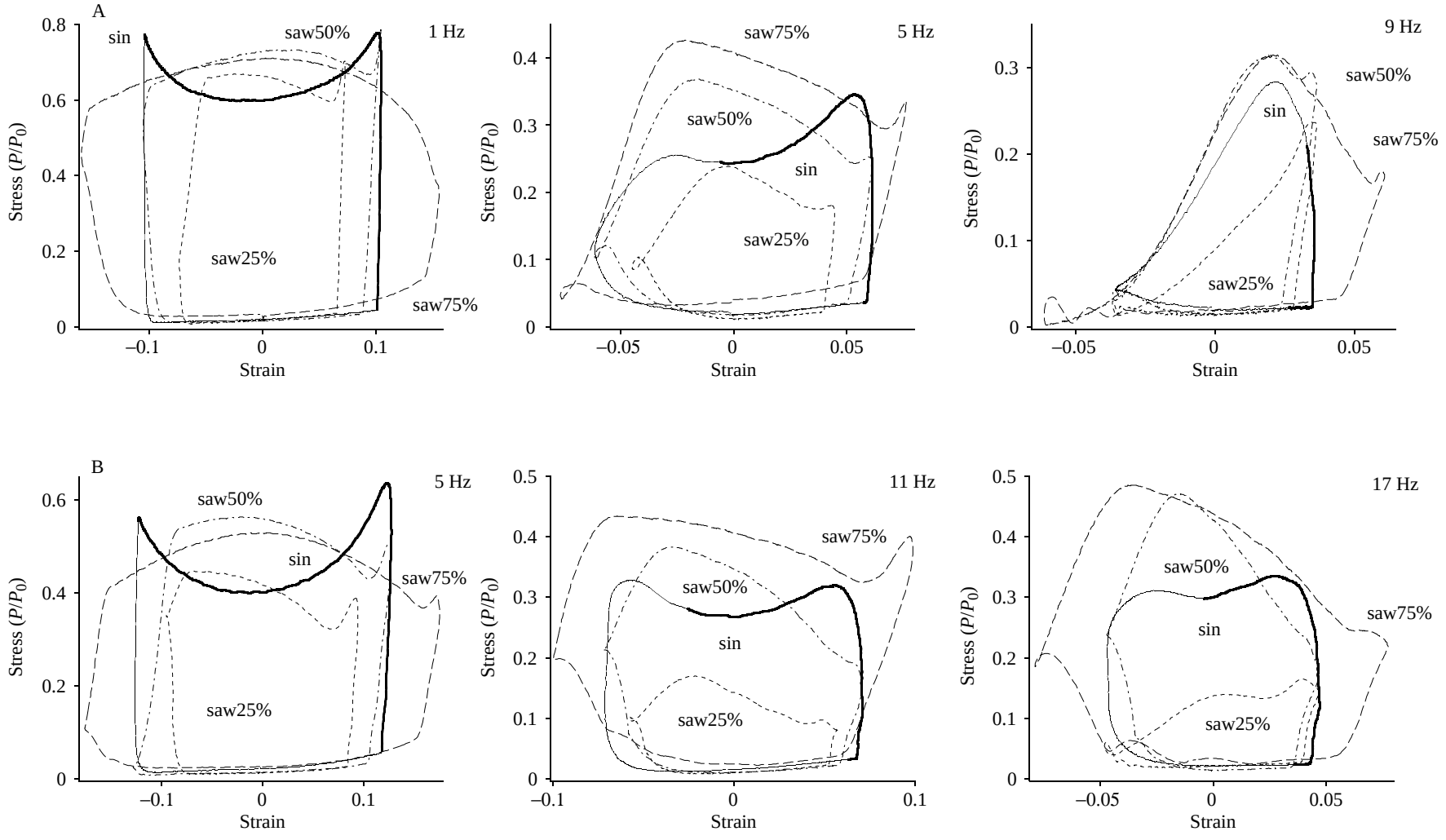


Fig. 7. Work loops plotted for different strain trajectories (see Fig. 2) over a range of cycle frequencies for (A) soleus and (B) EDL muscle. Isometric stress ($P_0$) and optimum muscle length ($L_0$) are as follows. (A) 1 Hz: 29.4 N cm$^{-2}$, 10.0 mm; 5 Hz: 28.8 N cm$^{-2}$, 9.0 mm; 9 Hz: 29.0 N cm$^{-2}$, 10.0 mm. (B) 5 Hz: 25.1 N cm$^{-2}$, 10.5 mm; 11 Hz: 24.6 N cm$^{-2}$, 10.0 mm; 17 Hz: 25.1 N cm$^{-2}$, 10.5 mm. The period for which the muscle was stimulated is shown (bold line) at each cycle frequency for the sinusoidal strain trajectory (stimulation for other length trajectories is not illustrated for clarity).

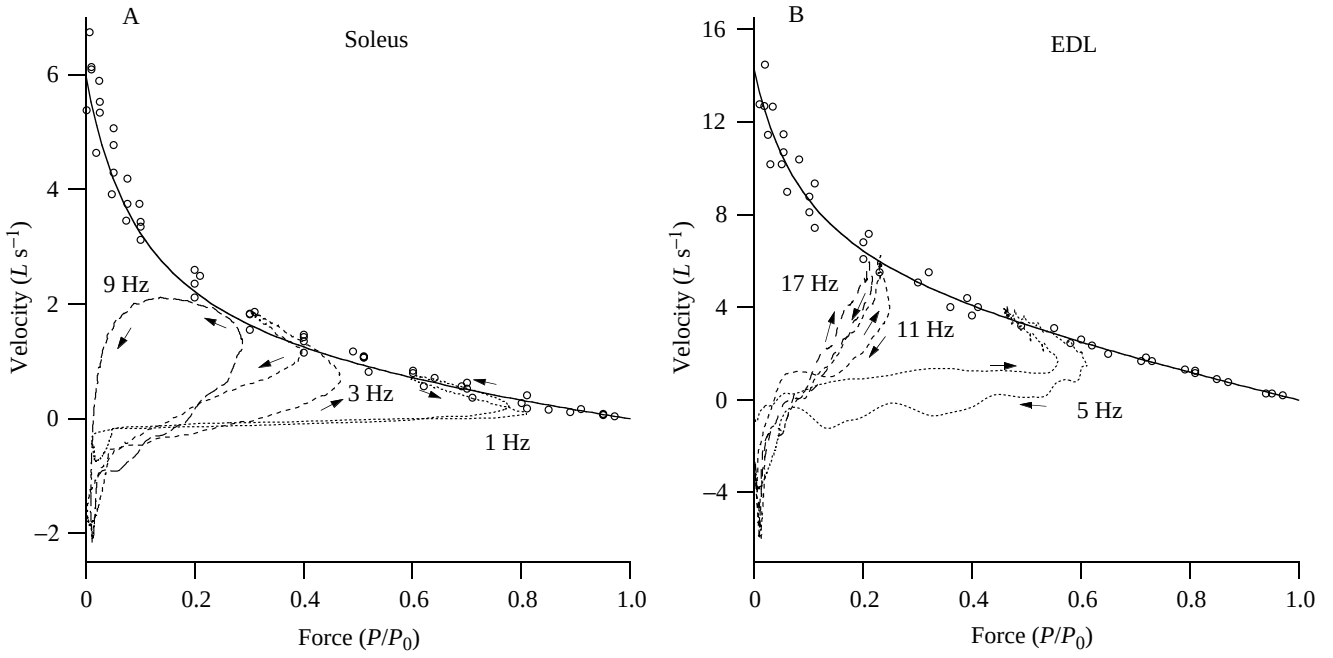


Fig. 8. Force–velocity relationships generated during after-loaded isotonic, tetanic contractions for mouse soleus (A) and EDL (B) muscle. A hyperbolic–linear function (Marsh and Bennett, 1986) has been fitted to the data based upon mean values for the constants *A*, *B* and *C* (from four muscles for each plot, open circles). Force–velocity data during sinusoidal strain cycles have been superimposed on the force–velocity relationship. Arrows indicate the direction of the loop.

because previous authors have not reported the fibre type composition of the muscles used. Not surprisingly, our results confirm that the soleus of the mouse is predominantly slow-twitch (type I) and the EDL is predominantly fast-twitch oxidative (type IIb). However, even though the fibre type distribution of these muscles is generally the same, previous studies reveal differences that are probably due to strain, sex and age. For example, Haida *et al.* (1989) found a lower percentage of the cross-sectional area of the soleus occupied by slow-twitch fibres than we did, but found a larger cross-sectional area of the EDL occupied by type IIb fibres. Substantial age (Wirtz *et al.* 1983) and sex (Stickland and O'Shaughnessy, 1994) differences in fibre type composition have also been documented. We suggest that future studies of the contractile properties of the muscles of laboratory animals recognise this variability and document fibre type composition to facilitate comparisons.

### *The effects of length trajectory on muscle power output*

Power was maximal at a distinct optimal cycle frequency (Fig. 4). Above and below this frequency, power declined. Similar findings have been reported for many other muscles studied using the work loop technique (for example, Stokes and Josephson, 1988; Altringham and Johnston, 1990; Swoap *et al.* 1993; James *et al.* 1995). When the proportion of the cycle spent shortening was held constant at 50 %, changing from a sinusoidal to a sawtooth length trajectory had only a small effect on the power output. These results are consistent with the predictions of the simple model of Josephson (1989), although his model did not consider activation and deactivation events. In most cases, force was highest during sinusoidal cycles at the start of shortening, which is consistent with force–velocity effects. However, the force during saw50% cycles exceeded that during sinusoidal cycles throughout most of shortening (Fig. 7).

The power output of both soleus and EDL increased at any given cycle frequency as the proportion of shortening increased from saw25% to saw75% (Fig. 4; Table 2). The power output at the optimal cycle frequency also increased, by approximately 2.5-fold, as the proportion of the cycle spent shortening increased from saw25% to saw75% (Fig. 4; Table 2). Results from a more limited data set at a single cycle frequency indicated that power output increased up to a shortening duration as high as 85–95 % of the cycle duration. Several factors promote the production of power as the proportion of the cycle spent shortening increases.

First, work is maximized at an optimal ratio of $V/V_{max}$, which is dependent on length trajectory (Fig. 6B) and cycle frequency (G. N. Askew and R. L. Marsh, unpublished observations). As the proportion of shortening increases at a particular cycle frequency, the strain amplitude must be increased to maintain an optimal $V/V_{max}$ (Figs 6, 7, 9). For example, the optimal strain amplitude for mouse soleus operating at 5 Hz increased from ±3 % using saw25% to ±9 % using saw75% strain trajectories. Work is the integral of force with respect to length; therefore, increasing the optimal strain amplitude enhances the power output of the muscle.

Second, during a cyclical contraction, a muscle must be

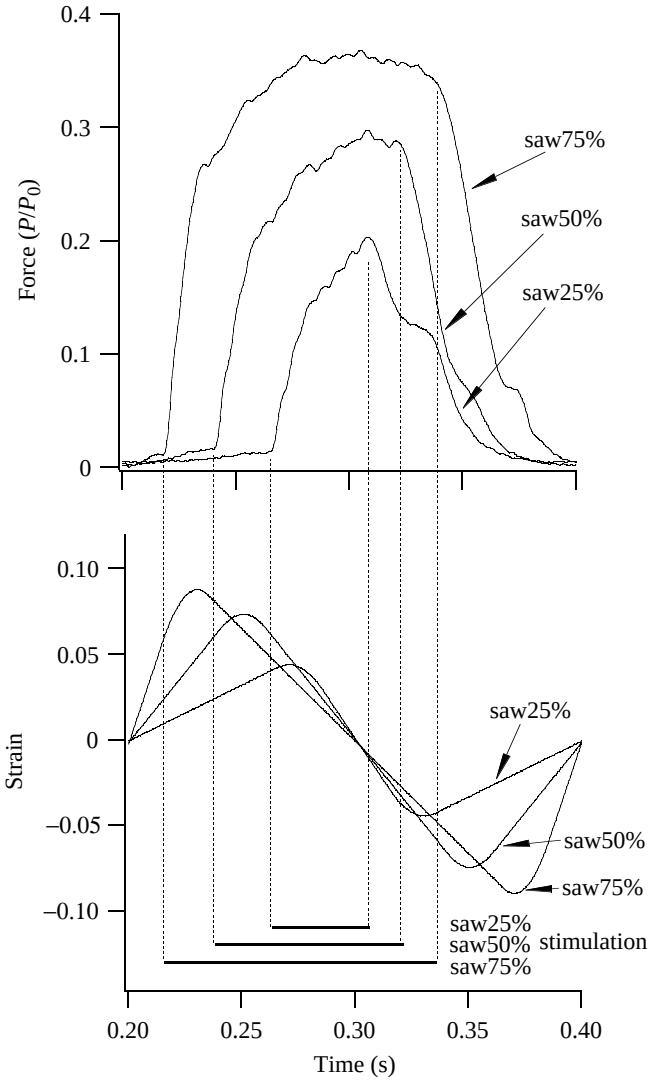


Fig. 9. Force and length trajectories for the soleus muscle operating at 5 Hz. The upper panel shows force developed during cyclical contractions using different sawtooth length trajectories (see Fig. 2). Below, the strain during three different length trajectories is shown, and the strain amplitude yielding maximum power is also illustrated. The duration of stimulation is illustrated by bars in the lower panel; broken lines have been extended to the upper panel. Isometric stress, $L_0$ and muscle mass were 27.6 N cm$^{-2}$, 10.0 mm and 5.0 mg, respectively. Work performed per cycle was 15.5 J kg$^{-1}$ (saw75%), 11.2 J kg$^{-1}$ (saw50%) and 4.5 J kg$^{-1}$ (saw25%).

activated and then deactivated. In order to maximize power output, the muscle should be activated as it approaches its maximum length during the lengthening phase of the cycle (a process facilitated by stretch, see below) and should be largely deactivated before shortening ends (Figs 7, 9). The time available for activation and deactivation increases as the proportion of the cycle spent shortening increases, allowing the stimulation duration to be increased. The muscle is therefore able to generate higher forces as a result of more complete activation (Figs 7, 9), thereby increasing its power output. Greater activation is particularly important at high cycle frequencies, where incomplete activation reduces the work output during shortening, and partial activation into lengthening requires work to re-stretch the muscle owing to the brief shortening period (Josephson, 1985*b*).

Finally, if the strain amplitude during shortening is optimized, increasing the proportion of the cycle spent shortening results in an increase in the velocity of stretch imposed on the muscle. To maximize the power output of the muscle, the muscle is stimulated during lengthening, such that forces are high at the onset of shortening. From plots of force with respect to time (Fig. 9), it can be seen that the rate of rise of force increased with stretch velocity. Similarly, during rapid stretches of tetanically contracting muscles, force rises more rapidly at higher velocities of stretch (Edman *et al.* 1978; Lombardi and Piazzesi, 1990). Reducing the time required for force development increases the net power output of the muscle.

### *Power compared during cyclical contractions and isotonic shortening*

Maximal power derived from the force–velocity relationship presumably represents the maximum instantaneous power output of the muscle, but this does not represent the average power output that the muscle can generate during cyclical contractions (Josephson, 1993). Average power output measured during sinusoidal work loops has been found to be approximately 30 % of the isotonic power (Stevens, 1993; Marsh and Olson, 1994). However, we have found that, by manipulating the length trajectory to one where a greater proportion of the cycle was spent shortening, the average power output obtained can be increased dramatically. For example, the soleus muscle generated 72 % of its isotonic power output using a saw85% length trajectory and the EDL generated 66 % of its isotonic power output using a saw95% length pattern (Fig. 5). It may be possible to increase power output somewhat above these values, as we did not determine the optimal cycle frequency for these length trajectories. However, on the basis of measurements for other length trajectories (Fig. 4), these cycle frequencies are likely to be close to optimal.

### *Optimal cycle frequency for maximum power output*

For each cyclical length pattern used, there was an optimum cycle frequency ($f_{opt}$) at which power was maximal, but the optimal frequency was influenced by the length trajectory. The optimal frequency and maximum power output of EDL were considerably greater than those of soleus (Fig. 4). The EDL generated higher levels of work at a given cycle frequency than the soleus because of its more rapid activation and deactivation kinetics and higher $V_{max}$. As the proportion of the cycle spent shortening increased, $f_{opt}$ also increased (Table 2; Fig. 4), because the muscle was able to perform more work at a particular cycle frequency and, as a result, the power–frequency relationship shifted to higher frequencies (Fig. 4; Table 2).

### *Work loop shape*

Work loop shapes varied among the different strain trajectories and also between the two muscles studied. During sinusoidal work loops, force rose towards the end of lengthening as a result of activation of the fibres, reaching a maximum at or shortly after the muscle's maximum length. Force then declined during shortening as velocity increased, consistent with force–velocity effects. At low cycle frequencies, force sometimes rose again as velocity decreased towards the end of shortening. However, at higher cycle frequencies, force continued to fall late in the shortening period because stimulation was stopped earlier in the cycle to avoid continued force production during lengthening and a reduction in net power output. The EDL, being a faster-contracting muscle (Table 1), was active throughout much of shortening at all of the cycle frequencies studied, resulting in 'U'-shaped work loops (Fig. 7). The soleus produced these U-shaped work loops only at low cycle frequencies. At higher frequencies, the muscle was only activated for part of the shortening phase and the loops were more 'triangular' in shape (Fig. 7).

Sawtooth work loops at low cycle frequencies tended to attain peak force midway through shortening (Fig. 7). At these low cycle frequencies, where optimal strain amplitudes were highest, the peak in force is consistent with the effects of the length–force relationship (Fig. 3). At higher frequencies, the force was much lower at the start and end of shortening, where the muscle was still activating and relaxing (Fig. 7). Again for the EDL, forces tended to remain higher throughout much of the shortening phase of the strain because less of the cycle was taken up with activating and deactivating the muscle compared with the soleus (Fig. 7).

### *The force–velocity trajectory during dynamic contractions*

The extent to which mouse soleus and EDL muscles operate on their force–velocity curves during dynamic contractions was examined by superimposing force and velocity recorded during sinusoidal work loops onto force–velocity curves measured during after-loaded isotonic, tetanic contractions (Fig. 8). Previous work has shown that the isotonic curve provides an approximate upper boundary to the force–velocity trajectory (Marsh and Olson, 1994). During activation and deactivation, the muscle produces submaximal force and operates below the force–velocity curve (Fig. 8). As the proportion of the cycle spent activating and deactivating is lowest at low cycle frequencies, muscles were found to operate for longest on their force–velocity curves at these frequencies.

Other studies have suggested that, during dynamic contractions, muscles may produce forces substantially higher that those predicted from the force–velocity relationship. Recently, it has been reported that the force generated during *in vitro* simulations of C-starts in an Antarctic fish *Notothenia coriiceps*, is 10 times greater than that predicted from the force–velocity relationship (Franklin and Johnston, 1997). Stevens (1993) found that forces generated by mouse soleus exceeded the force–velocity relationship by as much as 30 %. However, our data presented here for the same muscle, and also for the EDL, show that the muscle operates largely on or below the force–velocity curve. One hypothesis which would explain the force enhancement noted by other authors is that energy stored is in series elastic elements, including cross-bridges and connective tissue elements, prior to shortening. Using frog tibialis anterior muscles, Iwamoto *et al.* (1990) found that when force was ramped down from $P_0$ to zero, muscles operated above their steady-state force–velocity relationship. However, they also noted that these effects could be explained by the release of elastic strain energy from the series elastic component of the muscle (Iwamoto *et al.* 1990). Interestingly, in the scallop *Argopecten irradians* adductor muscle, where there is no tendon, force is produced predominantly on or below the force–velocity relationship during cyclical contractions (Marsh and Olson, 1994). In fish muscle, despite the huge enhancement of force above the force–velocity curve, the average cyclical power output of caudal myotomes during C-starts is relatively low because considerable work is absorbed during stretching prior to shortening (Franklin and Johnston, 1997). Also consistent with the above hypothesis, Stevens (1993) noted that force enhancement above the force–velocity relationship increased the earlier the muscle was stimulated before peak length. The earlier in the lengthening phase that a muscle is stimulated, the more negative work will be performed, which could potentially be stored elastically and released during the subsequent shortening period. According to this hypothesis, the differences between our results and those of Stevens (1993) could be explained if there was greater compliance in the muscles used by Stevens (1993), but we have no direct evidence of this difference.

### *Relationship to* in vivo *performance*

These experiments have clearly demonstrated that the net power output of skeletal muscles *in vitro* can be increased by increasing the proportion of shortening in the cycle (Fig. 4). We have shown that this improved performance occurs at all cycle frequencies and in both fast- and slow-twitch muscles. This leads to the intriguing conclusion that the performance of a reciprocating, muscularly driven system that requires high mass-specific power output can be improved by powering only one phase of the cycle. Clearly, the advantages that are offered by extending the shortening phase cannot be used in all systems involved in cyclical work *in vivo*, because morphological and biomechanical constraints may make it advantageous to spend equal times shortening and lengthening. For example, swimming in fish is powered by equally sized muscles that create alternate bending of the trunk. Nevertheless, we have found a number of examples that suggest that animals exploit prolonging the shortening phase to improve power output.

Many tree frogs make loud calls during the breeding season in order to attract mates. The power required to produce the call is provided by contraction of the internal and external oblique muscles, which forces air over the vocal chords. Air is returned to the lungs by the passive recoil of the distended

vocal sac. During such calls, the external oblique muscles shorten for 60 % (*Hyla chrysoscelis*) and 75 % (*H. versicolor*) of the length change cycle (Sarbadhikary and Marsh, 1995; Girgenrath and Marsh, 1997). *In vitro* measurements of power output during sinusoidal trajectories and simulated *in vivo* cycles revealed that, for both *Hyla* species, the external oblique muscles could generate over twice as much power during the natural cycles (M. Girgenrath and R. L. Marsh, unpublished observations).

Scallops propel themselves using jets of water formed by the closure of their two valves when the adductor muscle contracts. Opening is powered by energy stored in the hinge ligament during closing. During swimming, *Argopecten irradians* performs cyclical contractions during which the adductor muscle shortens for 56 % of the length change cycle (Marsh and Olson, 1994); in *Chlamys hastata*, which operates at a higher frequency and higher power output, the adductor muscle shortens for 65 % of the strain cycle (Marsh *et al.* 1992).

During slow, flapping flight in most birds and bats, the downstroke generates the lift required to support the body weight of the animal. The upstroke is much more lightly loaded because the wings are drawn in close to the body, and this phase is powered by much smaller antagonistic muscles. Kinematic data (Tobalske and Dial, 1996) and, more recently, sonomicrometry recordings (A. A. Biewener, personal communication) show that, during slow flight in the pigeon, the downstroke occupies 60–65 % of the wing stroke.

To conclude, we have demonstrated that, by increasing the proportion of the cycle time spent shortening, muscle power output can be increased. This increase occurs over the whole range of cycle frequencies that we studied, both above and below that yielding maximum power output and for both predominantly slow- and fast-twitch muscles. At cycle frequencies below $f_{opt}$, power output can also be increased by increasing the operating frequency. However, even at the lowest cycle frequencies that we studied, the power output of the saw75% cycles was higher than the maximum power during sinusoidal cycles. At cycle frequencies above $f_{opt}$, the power output cannot be increased by increasing frequency, and manipulating the length trajectory is the only known mechanism by which power can be dramatically increased. By changing the length trajectory in this way, muscles may be able to operate at higher cycle frequencies than would be possible using symmetrical strain cycles. In an evolutionary context, increasing the relative shortening duration is an alternative to increasing $V_{max}$. The possible influence of altering the length trajectory on endurance and efficiency remains to be explored.

This work was supported by grant AR39318 awarded by the NIH to R.L.M.

## References

ALTRINGHAM, J. D. AND JOHNSTON, I. A. (1990). Modelling muscle power output in a swimming fish. *J. exp. Biol.* **148**, 395–402.

CHAN, W. P. AND DICKINSON, M. H. (1996). *In vivo* length oscillations of indirect flight muscles in the fruit fly *Drosophila virilis*. *J. exp. Biol.* **199**, 2767–2774.

CHAYEN, J. AND BITENSKY, L. (1991). *Practical Histochemistry*, second edition. pp. 164–166. Chichester: John Wiley & Sons.

CLOSE, R. I. (1964). Dynamic properties of fast and slow muscles of the rat during development. *J. Physiol., Lond.* **173**, 74–95.

CLOSE, R. I. (1972). Dynamic properties of mammalian skeletal muscles. *Physiol. Rev.* **52**, 129–197.

COUGHLIN, D. J., VALDES, L. AND ROME, L. C. (1996). Muscle length changes during swimming in scup: sonomicrometry verifies the anatomical high-speed cine technique. *J. exp. Biol.* **199**, 459–463.

DAUT, J. AND ELZINGA, G. (1989). Substrate dependence of energy metabolism in isolated guinea-pig cardiac muscle: a microcalorimetric study. *J. Physiol., Lond.* **413**, 379–397.

EDMAN, K. A. P., ELZINGA, G. AND NOBLE, M. I. M. (1978). Enhancement of mechanical performance by stretch during tetanic contractions of vertebrate skeletal muscle fibres. *J. Physiol., Lond.* **281**, 139–155.

FRANKLIN, C. E. AND JOHNSTON, I. A. (1997). Muscle power output during escape responses in an Antarctic fish. *J. exp. Biol.* **200**, 703–712.

GILMOUR, K. M. AND ELLINGTON, C. P. (1993). *In vivo* length changes in bumblebees and the *in vitro* effects on work and power. *J. exp. Biol.* **183**, 101–113.

GIRGENRATH, M. AND MARSH, R. L. (1997). *In vivo* performance of trunk muscles in tree frogs during calling. *J. exp. Biol.* **200**, 3101–3108.

HAIDA, N., FOWLER, W. M., JR, ABRESCH, R. T., LARSON, D. B., SHARMAN, R. B., TAYLOR, R. G. AND ENTRIKIN, R. K. (1989). Effect of hind-limb suspension on young and adult skeletal muscle. I. Normal mice. *Exp. Neurol.* **103**, 68–76.

IWAMOTO, H., SUGAYA, R. AND SUGI, H. (1990). Force–velocity relation of frog skeletal muscle fibres shortening under continuously changing load. *J. Physiol., Lond.* **422**, 185–202.

JAMES, R. S., ALTRINGHAM, J. D. AND GOLDSPINK, D. F. (1995). The mechanical properties of fast and slow skeletal muscles of the mouse in relation to their locomotory function. *J. exp. Biol.* **198**, 491–502.

JOSEPHSON, R. K. (1985*a*). Mechanical power output from striated muscle during cyclical contractions. *J. exp. Biol.* **114**, 493–512.

JOSEPHSON, R. K. (1985*b*). The mechanical power output of a tettigoniid wing muscle during singing and flight. *J. exp. Biol.* **117**, 357–368.

JOSEPHSON, R. K. (1989). Power output from skeletal muscle during linear and sinusoidal shortening. *J. exp. Biol.* **147**, 533–537.

JOSEPHSON, R. K. (1993). Contraction dynamics and power output of skeletal muscle. *A. Rev. Physiol.* **55**, 527–546.

JOSEPHSON, R. K. AND ELLINGTON, C. P. (1997). Power output from a flight muscle of the bumblebee *Bombus terrestris*. I. Some features of the dorso-ventral flight muscle. *J. exp. Biol.* **200**, 1215–1226.

JOSEPHSON, R. K. AND STOKES, D. R. (1989). Strain, muscle length and work output in a crab muscle. *J. exp. Biol.* **145**, 45–61.

LAYLAND, J., YOUNG, I. S. AND ALTRINGHAM, J. D. (1995). The length-dependence of work production in rat papillary muscles *in vitro*. *J. exp. Biol.* **198**, 2491–2499.

LOMBARDI, V. AND PIAZZESI, G. (1990). The contractile response during steady lengthening of stimulated frog muscle fibres. *J. Physiol., Lond.* **431**, 141–171.

LUFF, A. R. (1981). Dynamic properties of the inferior rectus, extensor

digitorum longus, diaphragm and soleus muscles of the mouse. *J. Physiol., Lond.* **313**, 161–171.

MARSH, R. L. AND BENNETT, A. F. (1986). Thermal dependence of contractile properties of skeletal muscle from the lizard *Sceloporus occidentalis* with comments on methods for fitting and comparing force–velocity curves. *J. exp. Biol.* **126**, 63–77.

MARSH, R. L. AND OLSON, J. M. (1994). Power output of scallop adductor muscle during contractions replicating the *in vivo* mechanical cycle. *J. exp. Biol.* **193**, 139–156.

MARSH, R. L., OLSON, J. M. AND GUZIK, S. K. (1992). Mechanical performance of scallop adductor muscles during swimming. *Nature* **357**, 411–413.

NACHLAS, M., TSOU, K. C., DESOUZA, E., CHEUNG, C. S. AND SELIGMAN, A. M. (1957). Cytochemical demonstration of succinate dehydrogenase by the use of a new p-nitrophenol substituted ditetrazole. *J. Histochem. Cytochem.* **5**, 420–436.

PADYKULA, H. AND HERMAN, E. (1955). The specificity of the histochemical method for adenosine triphosphate. *J. Histochem. Cytochem.* **3**, 170–195.

RACK, P. M. H. AND WESTBURY, D. R. (1969). The effects of length and stimulus rate on tension in the isometric cat soleus. *J. Physiol., Lond.* **204**, 443–460.

ROBERTS, T. J., MARSH, R. L., WEYAND, P. G. AND TAYLOR, C. R. (1997). Muscular force in running turkeys: the economy of minimizing work. *Science* **275**, 1113–1115.

SARBADHIKARY, M. AND MARSH, R. L. (1995). *In vivo* performance of trunk muscles in tree frogs during calling. *Am. Zool.* **35**, 141A.

STEVENS, E. D. (1993). Relation between work and power calculated from force–velocity curves, to that done during oscillatory work. *J. Muscle Res. Cell Motil.* **14**, 518–526.

STICKLAND, N. C. AND O'SHAUGHNESSY, P. J. (1994). The influence of male-specific genes on female muscle fibre types: studies on the sex-reverses (Sxr) mouse. *J. exp. Zool.* **269**, 378–382.

STOKES, D. R. AND JOSEPHSON, R. K. (1988). The mechanical power output of a crab respiratory muscle. *J. exp. Biol.* **140**, 287–299.

SWOAP, S. J., JOHNSON, T. P., JOSEPHSON, R. K. AND BENNETT, A. F. (1993). Temperature, muscle power output and limitations on burst performance of the lizard *Dipsosaurus dorsalis. J. exp. Biol.* **174**, 185–197.

SYME, D. A. AND JOSEPHSON, R. K. (1995). Influence of muscle length on work from trabecular muscle of frog atrium and ventricle. *J. exp. Biol.* **198**, 2221–2227.

TOBALSKE, B. W. AND DIAL, K. P. (1996). Flight kinematics of black-billed magpies and pigeons over a wide range of speeds. *J. exp. Biol.* **199**, 263–280.

WIRTZ, P., LOERMANS, H. M., PEER, P. G. AND REINTJES, A. G. (1983). Postnatal growth and differentiation of muscle fibres in the mouse. I. A histochemical and morphometrical investigation of normal muscle. *J. Anat.* **137**, 109–126.